ELSEVIER

Quantitative evaluation of the surface stability and morphological changes of Cu$_2$O particles

Mateus M. Ferrer [a], Guilherme S.L. Fabris [b], Bruno V. de Faria [b], João B.L. Martins [c], Mário L. Moreira [a], Julio R. Sambrano [b],*

[a] Department of Physics, Federal University of Pelotas, UFPel, 96160-000, Pelotas, RS, Brazil
[b] Modeling and Molecular Simulations Group, São Paulo State University, UNESP, 17033-360, Bauru, SP, Brazil
[c] Computational Chemistry Laboratory, University of Brasilia, 70904-970, Brasília, DF, Brazil

ARTICLE INFO

ABSTRACT

Cu$_2$O low-index surfaces periodic models have been simulated based on density functional theory. The calculated surfaces energies allowed estimating the morphology by means of the Wulff theorem as well as the investigation of possible paths of morphological changes. Therefore, systematic morphology diagrams and change paths according to the energy modulation in relation to the surfaces stabilizations were elaborated. The applicability of this strategy was exemplified by comparing the obtained results with experimental available data from the literature. The morphology diagrams with the quantitative energetic point of view can be used as a guide to support experimental works in order to understand the relation between surface interactions and crystal growth.

1. Introduction

During the last decades, intensive efforts have been employed in the synthesis of crystalline materials with tailored shapes and different properties attributed to different exposed surfaces [1, 2, 3]. The energy excess and the energy distribution on the surfaces are important topics to be explored when it comes to understanding the growth and stability/activity of particles, mainly in the nanometric scale [4, 5]. In this sense, quantum mechanical simulations have been presented concepts and explanations that experimental approach has difficult in achieving [6, 7]. Even that the theoretical studies have been shown enlightening trends, there are still several open questions about the mechanisms that govern the modulation of the surfaces making it an open field of research. Therefore, the correlation of theoretical approaches with experimental evidence can be considered as an interesting way to the development of models that simplify the development of materials with desired properties.

In the particular case of morphological studies, it is important to emphasize that particles formed by different facets with distinctive crystallographic indices can generate characteristics/properties totally different. These studies include differences of the surface terminations, the atomic unsaturation, and the atomic and electron density of a plane, which reflects directly on properties as catalysis, sensing and conductivity [8, 9, 10]. Therefore, even for particles with apparently similar morphology, a slightly different inclination of one of the faces needs to be evaluated.

In this context, copper (I) oxide (Cu$_2$O) particles have recently attracted attention due to the morphology-dependent applications [11, 12]. The new theoretical-experimental approaches showed the great diversity of how this material can present itself [11, 13].

The Cu$_2$O is usually a p-type semiconductor with a band gap of ~2.2 eV with unique optical, electrical and magnetic properties [14, 15]. In addition, it has a low cost, is non-toxic and is abundantly available [11]. This solid is known for crystallizing itself in a cubic structure with space group *Pn*-3*m* usually interpreted as two sub-lattice, where four Cu$^+$ cations are located on a face-centered cubic (*fcc*) sub-lattice while the two O^{2-} ions are in the body-centered cubic (*bcc*) sub-lattice, occupying two of the tetragonal sites. This structure results in all Cu ions bicoordinated with O ions and all O ions tetracoordinated with Cu ions. A unit cell scheme can be seen in Fig. 1.

---

* Corresponding author.
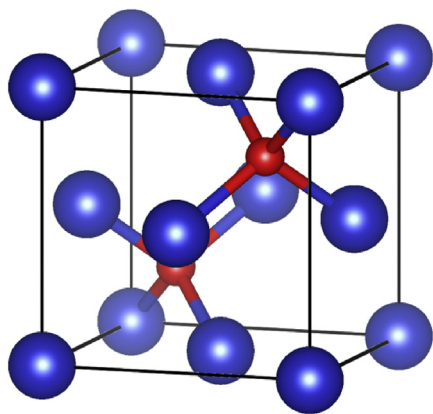 *E-mail address:* jr.sambrano@unesp.br (J.R. Sambrano).

Fig. 1. Unit cell scheme of the Cu_2O. (Red and blue colors represent the O and Cu atoms, respectively).

Besides these properties and characteristics, Cu_2O has been showing potential of application as a catalyst of different species, energy conversion processes and sensing [11, 16]. Thus, it is undoubted the importance of a systematic detailing of Cu_2O surface when discussing the properties previously mentioned.

In summary, Cu_2O is considered as a material composed of particles with easily moldable form. This makes this material an interesting example of how the form can be directly related to the properties at equilibrium [17, 18]. There is a great number of studies that report a great diversity of morphologies of this system, especially in cubic, octahedral and rhombic dodecahedral crystals [19, 20]. It may be noted that the major structures in equilibrium are obtained with the combination of the (100), (111), and (110) low-index exposed facets. This fact shows the high stability of the low-index in comparison with other high-index cut planes to the Cu_2O structure.

Scientific evidence show several ways of how the Cu_2O is susceptible to morphological changes as a function of the synthesis method [11, 12, 20, 21, 22]. Several facet-controlled routes can be found at literature with a great diversity of precursors, solvents and heating source [12, 20]. Besides that, small adjustments in some synthesis routes, such as the changes of surfactant concentration [21], pH [23], temperature [22] and reaction time [24], induce morphological changes due to the stabilization/destabilization of each surface in different orders.

In previous published articles, we have theoretically evaluated the morphological modification of metal oxides in relation to the stability of the surface [25, 26]. This methodology can provide useful quantitative information about the energetic modulation of the surface energy and the relationship among the control synthesis method, morphology and respective properties.

The present study performs quantum computational calculations to explore surface models of Cu_2O low-index planes. The results of the models were also applied to study all possible morphological changes in a quantitative point of view in respect to the energy modulation. Such information was organized in the form of diagrams that brings the possibility of a direct comparison with experimental results in order to provide explanations about the particles growth directions under different experimental conditions.

2. Methodology

Quantum mechanical calculations were performed according to density functional theory (DFT) in conjunction with PBE functional implemented in Vienna ab initio simulation (VASP) package (Version 5.4.1) [27, 28, 29]. The atomic basis set was described by the projector-augmented-wave pseudo-potentials [27, 30]. In addition, it was used a cut-off energy of 520 eV and Monkhorst-Pack scheme to the k-points grid (5×5×5). In the first step of the calculations, it was

performed a structural optimization of the cubic Cu_2O in order to achieve the global minimum energy. The structural parameters of the input data were extracted from the Inorganic Crystal Structure Database (ICSD) CARD 63281 [31]. The structure optimization yielded a unit cell expansion where the lattice parameters changed from 4.267 Å to 4.314 Å. In addition, the estimated band gap energy was 0.48 eV, a value already expected due to the underestimation caused by the PBE functional. The band structure and the projected density of states (DOS) of the optimized bulk are shown in Figs. 2 and 3, respectively.

The (100), (110) and (111) surfaces were modeled from the optimized bulk parameters taking into account the dipole corrections. A 15 Å vacuum spacing was added between the surfaces in order to prevent interaction with each other. The slab models were optimized with the relaxation of all atoms of the structure.

It was performed calculations with all possible terminations of stoichiometric structures without reconstruction. The surface Energy (E_{surf}) values were calculated as performed in previous papers [25, 26, 32]. In addition, the thickness of each surface was select in a way to reach the convergence of the corresponding surface energy. This procedure is intended to include the bulk properties in the model and to represent an equilibrium condition.

The surface energy calculations allowed the estimation of the ideal particle morphology at a fixed volume by means of the Wulff theory, which relates the surface energies with the distance of the surface in a perpendicular direction from the center of the bulk [33]. The Wulff crystals were constructed by means of the VESTA program [34].

The study of the dangling bond density (Db) was also performed to a direct comparison with the theoretical results and to improve the exploration of each surface. The (Db) was calculated using Eq. (1), where Nb is the number of dangling bonds per unit cell area on a particular surface and A is the area of the surface unit cell [35, 36].

$$D_b = \frac{N_b}{A} \qquad (1)$$

3. Results and discussion

Fig. 4 shows a side view scheme of the selected (100), (110) and (111) slabs. These terminations showed the most stable surface (lowest surface energy) between all stoichiometric configurations in our models.

As shown in Fig. 4, the (100) surface presents just one possibility of the ideal and stoichiometric surface. In this condition, one side is O-terminated while the opposite side is Cu-terminated. It is worth noting
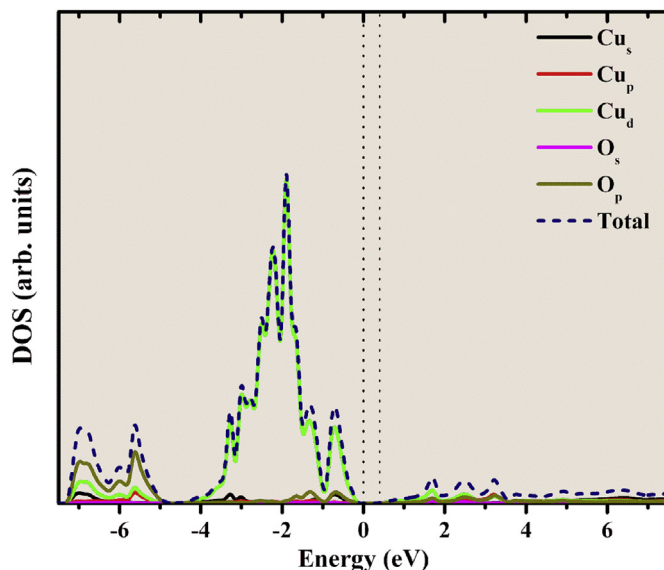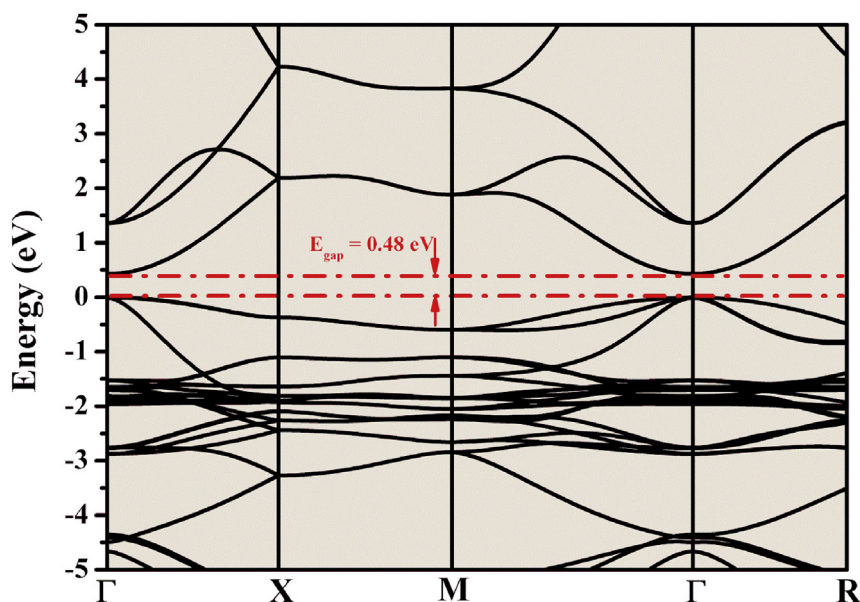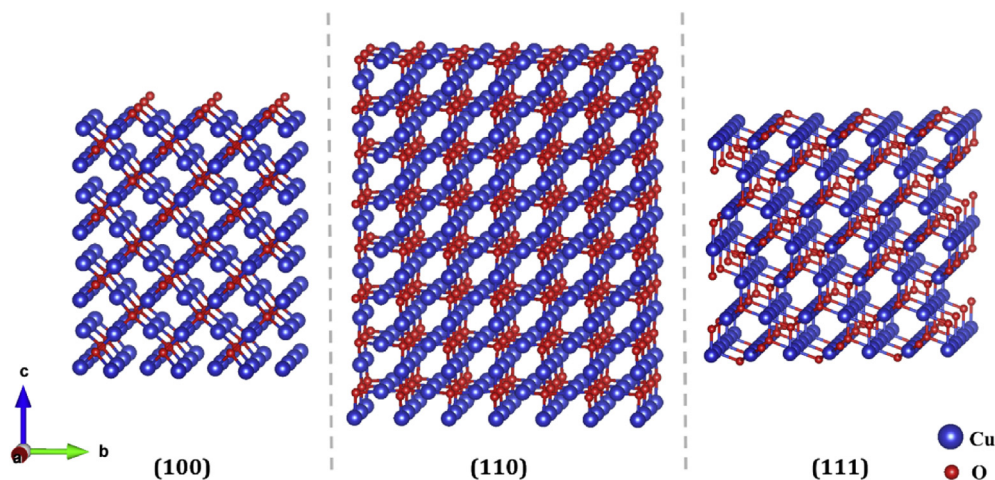

Fig. 2. Projected density os state of Cu2O bulk.

Fig. 3. Band structure of Cu_2O bulk.

Fig. 4. Side view of the (100), (110) and (111) slabs.

that the Cu-terminated surface is composed of two different Cu sites resulting in twice as many Cu as exposed Oxygen found in the opposite surface. The (110) surface also presents only one possibility of perfect and stoichiometric surface, Cu-terminated and CuO-terminated surfaces. The CuO-terminated side is composed of just one Cu site resulting in an equal ratio of Cu and O atoms. In the case of the (111) surface, two different terminations are possible in the perfect surfaces. The condition of the O-terminated surface of both sides, represented in Fig. 4, presented the most stable condition. The convergence of (100), (110) and (110) E_{surf}'s were achieved with the use of 16 (n = 4), 16 (n = 8) and 21 (n = 7) layers, respectively. The total DOS of each slab model are presented in Fig. 5.

The biggest difference between the total DOS of the surface models (Fig. 5) was the absence of any band gap region of the (110) slab, which suggests this superficial unsaturation generates bands that cover the forbidden zone.

The surfaces energies values found in the Cu_2O models without and with the surface atoms relaxation (unrelaxed and relaxed) are listed in Table 1.

According to the E_{surf} found in Table 1, the calculated stability order of the surfaces was (111) > (110) > (100) for both unrelaxed and relaxed models.

For a better understanding of the stability issues of these surfaces, it was performed a count of the unsaturation numbers of the ion presented at the surfaces in order to evaluate their dangling bonds density. This simple method is known for showing adequate results regarding stability order for bivalent systems of simple structure since all structure is composed of similar interactions. Table 2 presents a detailed number of unsaturated ions of the top and bottom side of each slab model. The "double" term in Table 2 represents double unsaturated ions.

As described before, the saturated Cu ions are bicoordinated while O ions are tetracoordinated. Thus, it was found that the sum of the unsaturations of all studied slabs is 4, as presented in Tables 1 and 2. The D_b values show the (111) and (100) presented the lowest and the highest density of unsaturation, respectively. This result represents the same order of stability of the quantum simulations, showing an expected relation between the D_b and surface energy. Moreover, the energy surface is related to the number of formed dangling bonds.

From the calculated surfaces energies values (Table 1), it was generated the morphologies of the unrelaxed and relaxed system using the Wulff construction method in a vacuum condition, as presented in Fig. 6.
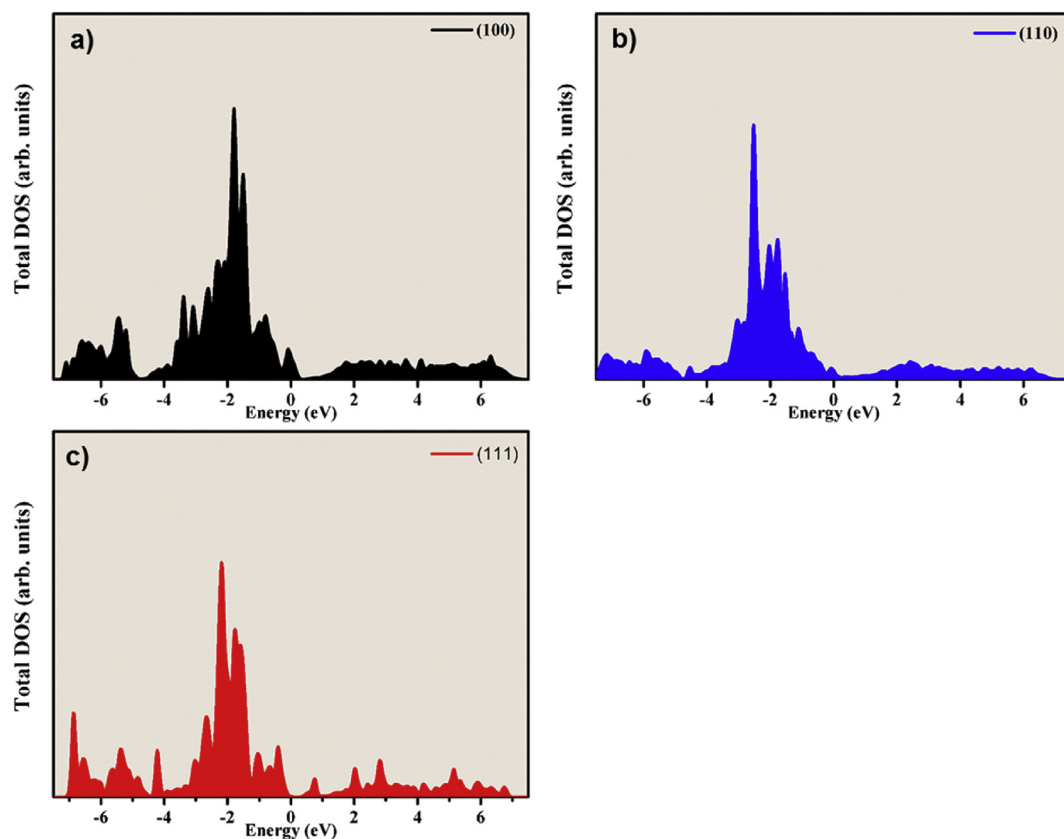
Fig. 5. Total density of states of the a) 100, b)110 and c)111 Cu_2O surface models.

Table 1
Surfaces energies and dangling bond density for Cu_2O surfaces.

Surface	E_{surf} unrelaxed (Jm^{-2})	E_{surf} relaxed (Jm^{-2})	Nb	Area (10^{-10} m^2)	Db
(100)	1.68	1.26	4	18.61	0.21
(110)	1.21	1.04	4	26.32	0.15
(111)	0.81	0.76	4	37.22	0.11

The relaxation method did not result in expressive changes in the Cu_2O morphology, as seen in Fig. 6. The unique observed change was the decrease of the (100) exposed area in relation of (111). In both cases, the surface energy value of (110) surface indicated that it is not low enough, or stable enough, for this surface to contribute to the Wulff solid. It is important to emphasize that the classic Wulff method does not allow predicting the differences of the particles size, but only allows predicting the relative exposed area between the surfaces. The octahedral estimated morphology is one of the most common morphology assumed by experimental particles, as cited before.

Starting from the ideal morphology, it is possible to modulate the E_{surf} of the studied surfaces in order to indicate paths of morphological changes. Fig. 7 presents the diagram for Cu_2O when the (100) and (110) stabilize separately and when both stabilize simultaneously.

The used method for the elaboration of the paths of Fig. 7 can be of great value to the understanding of the experimental changes observed in the Cu_2O system. The direct simulation of the real system, which considers all experimental variables, presents a great complexity due to the number of variables, both known and unknown. In addition, each experimental synthesis method, or even adjustments in a specific method, would require that new parameters and variables were taken into account for a new theoretical modeling. A general diagram with all possible morphologies, as presented here, is a way to circumvent the several variables of the reaction environment.

It is important to emphasize that would be possible to elaborate morphologies paths between any of intermediated morphology presented in Fig. 7. In order to show all possible morphologies with the (100), (110) and (111) faces combinations, Fig. 8 presents a path starting from the cubic (100) to the dodecahedral (110) particle of Fig. 7 keeping constant the E_{surf} of the (111) surface.

Some examples can be presented to show the functionality of diagrams. According to Xu and coworkers [21], the different conditions to reduce the $Cu(OH)_2$ to the formation of Cu_2O results in different final morphologies. The combination of Sodium ascorbate (1 mL, 0.1 mol/L) in Argon atmosphere resulted in a cubic morphology while the Hydrazine hydrate (0.06 mL, 85%) in Air atmosphere resulted in octahedrons. With results presented in (100) stabilization path in Fig. 7, it is possible to estimate that the Ar/Sodium ascorbate combination and sub-products in the environment induces the (100) stabilization decreasing its surface energy in a minimum of 0.52 (100)/(111) ratio. On the other hand, the Air/Hydrazine hydrate induces the (111) stabilization with the inverse of the first condition as a minimum value. A more detailed process of the (100)/(111) path can be observed in the Susman and coworkers study [37]. Looking at their paper and comparing with Fig. 7, the increase of 0.67–1.35 mL of sodium citrate (Na_3Cit) changed the (100)/(111) E_{surf} ratio of 1.66 to 0.79. This represents an energy stabilization of (100)
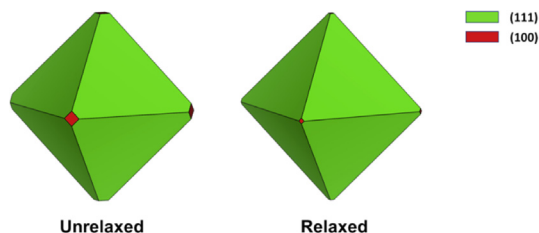

Fig. 6. Wulff crystals of the unrelaxed and relaxed structure of Cu_2O.

Table 2
Unsaturation count of the (100), (110) and (111) surfaces.

Planes	Oxygen		Oxygen N_b	Copper		Copper N_b	Total N_b
	Single	Double		Single	Double		
100							
Top	0	1	2	0	0	0	2
Bottom	0	0	0	2	0	2	2
Sum	0	1	2	2	0	2	4
110							
Top	2	0	2	0	0	0	2
Bottom	0	0	0	2	0	2	2
Sum	2	0	2	2	0	2	4
111							
Top	1	0	1	1	0	1	2
Bottom	1	0	1	1	0	1	2
Sum	2	0	2	2	0	2	4

Surface	E_{surf} (Jm^{-2})
(100)	1.26
(110)	1.04
(111)	0.76
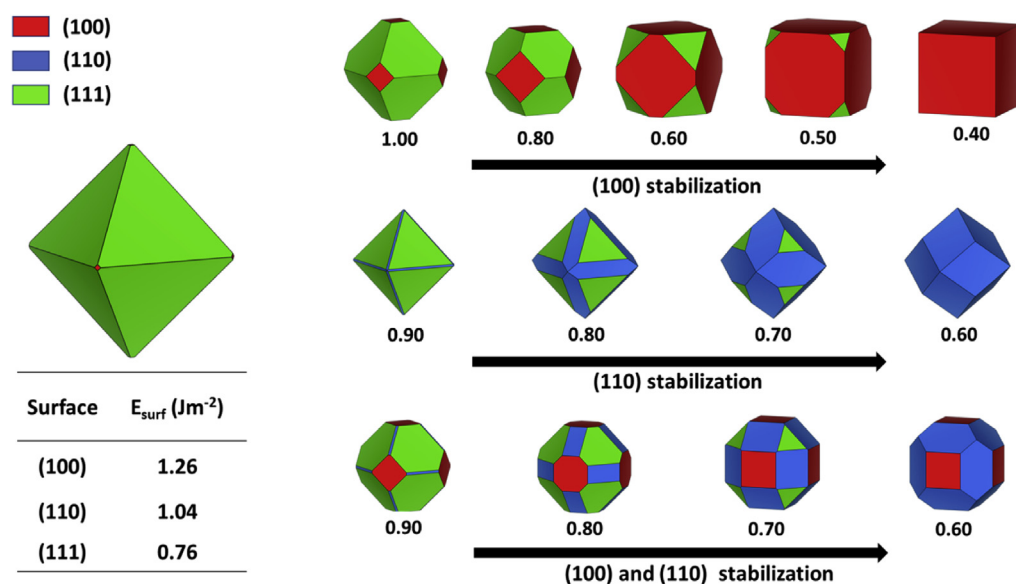
Fig. 7. Morphology diagram according to surfaces energy modulations.

surface caused by the Ni$_3$Cit higher than 100% in comparison to (111) surface. Subsequently, the authors increased the concentration of the Na$_3$Cit and decreased NaOH volume, in some stages, in order to find a cubic morphology. These last modulations represent a minimum of E_{surf} ratio change of 0.79 to 0.52, a minimum of 34.18% of (100) surface stabilization in comparison to the (111) surface. These results can clarify the rates of stabilizations caused by different amount of each species in the reaction environment.

The paper of Chen et al. [12] reports a great set of Cu$_2$O morphologies that can be found inside the morphologies diagrams. Among the reported morphologies, Chen shows that the concentration of Cl$^-$ ions in the glucose hydrothermal route controls the final morphology. The path of these changes represents the same observed in Fig. 7 with the (110) stabilization. With Cl$^-$ concentration used in the synthesis and the diagram of Fig. 7 in hands, it is possible to evaluate directly the relation of the amount of Cl$^-$ in solution and the (110) surface stabilization, as well as it was done in the previous example.

Other studies show examples where the morphology changes correspond to other morphologies found in Figs. 7 and 8 [11, 19, 38]. Furthermore, these other examples can be directly compared with the Cu$_2$O diagrams. This simple way of comparing the E_{surf} of each surface of Wulff crystal point of view represents a great facility as a first observation to the experimentalist when preparing Cu$_2$O with different morphologies.

4. Conclusions

In summary, we elaborated the bulk and surface models of Cu$_2$O by means of DFT/PBE calculations. The stoichiometric low index surface models indicated the following surface energy order: (111) < (100) < (100). The estimated dangling bonding densities also corroborated the energy order of the models.

Subsequently, theoretical morphology in equilibrium condition was estimated by means of simple Wulff methodology using the calculated surfaces energies. The obtained Wulff crystal of the ideal structure presented an orthorhombic morphology, in accordance with reported studies found in the literature that show this morphology is one of the most common for this system.

Starting from the estimated Wulff crystal shape, morphologies diagrams that show possible paths of morphological changes were elaborated according to different surface stabilizations. The use of this strategy presents a set of utilities in experimental approaches related to the morphology modulation. As an example of the utility of this strategy, the diagrams were used to evaluate the surface energy ratios observed in experimental particles as well as the energies involved in the morphologies modifications caused by differences in the synthesis methods. Therefore, morphology diagrams schemes represent an easy tool to assist in the quantitative understanding of modifications in experimental synthesis and in particles growth direction.
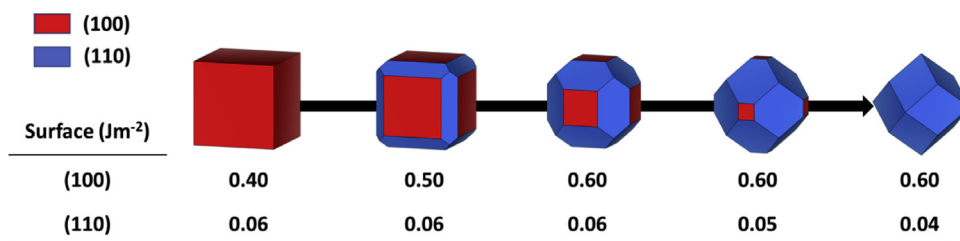
Fig. 8. Morphology modulation from the cubic to dodecahedron morphology.

Declarations

Author contribution statement

Mateus M. Ferrer: Conceived and designed the experiments; Performed the experiments; Analyzed and interpreted the data; Wrote the paper.

Guilherme S. L. Fabris: Conceived and designed the experiments; Performed the experiments; Analyzed and interpreted the data.

Bruno V. de Faria: Performed the experiments; Analyzed and interpreted the data; Wrote the paper.

João B. L. Martins: Analyzed and interpreted the data; Contributed reagents, materials, analysis tools or data; Wrote the paper.

Mário L. Moreira: Analyzed and interpreted the data.

Julio R. Sambrano: Conceived and designed the experiments; Analyzed and interpreted the data; Contributed reagents, materials, analysis tools or data; Wrote the paper.

Competing interest statement

The authors declare no conflict of interest.

Additional information

No additional information is available for this paper.

References

[1] C.Z. Wen, H.B. Jiang, S.Z. Qiao, H.G. Yang, G.Q.(Max, Lu, Synthesis of high-reactive facets dominated anatase TiO2, J. Mater. Chem. 21 (2011) 7052–7061.

[2] C. Wang, H. Daimon, T. Onodera, T. Koda, S. Sun, A general approach to the size- and shape-controlled synthesis of platinum nanoparticles and their catalytic reduction of oxygen, Angew. Chem. Int. Ed. 47 (2008) 3588–3591.

[3] Z. Wu, S. Yang, W. Wu, Shape control of inorganic nanoparticles from solution, Nanoscale 8 (2016) 1237–1259.

[4] Z.Y. Zhou, N. Tian, J.T. Li, I. Broadwell, S.-G. Sun, Nanomaterials of high surface energy with exceptional properties in catalysis and energy storage, Chem. Soc. Rev. 40 (2011) 4167–4185.

[5] Y. Jun, J. Choi, J. Cheon, Shape control of semiconductor and metal oxide nanocrystals through nonhydrolytic colloidal routes, Angew. Chem. Int. Ed. 45 (2006) 3414–3439.

[6] Z.W. Seh, J. Kibsgaard, C.F. Dickens, I. Chorkendorff, J.K. Nørskov, T.F. Jaramillo, Combining theory and experiment in electrocatalysis: insights into materials design, Science 355 (2017), eaad4998.

[7] A. Jain, Y. Shin, K.A. Persson, Computational predictions of energy materials using density functional theory, Nat. Rev. Mater. 1 (2016) 15004.

[8] C.S. Tan, S.C. Hsu, W.H. Ke, L.J. Chen, M.H. Huang, Facet-dependent electrical conductivity properties of Cu2O crystals, Nano Lett. 15 (2015) 2155–2160.

[9] Q. Hua, T. Cao, X.K. Gu, J. Lu, Z. Jiang, X. Pan, L. Luo, W.X. Li, W. Huang, Crystal-plane-controlled selectivity of Cu2O catalysts in propylene oxidation with molecular oxygen, Angew. Chem. Int. Ed. 53 (2014) 4856–4861.

[10] A. Gurlo, Nanosensors: towards morphological control of gas sensing activity. SnO2 , In2O3 , ZnO and WO3 case studies, Nanoscale 3 (2011) 154–165.

[11] Y. Shang, L. Guo, Facet-controlled synthetic strategy of Cu2O-based crystals for catalysis and sensing, Adv. Sci. 2 (2015) 1500140.

[12] K. Chen, C. Sun, D. Xue, Morphology engineering of high performance binary oxide electrodes, Phys. Chem. Chem. Phys. 17 (2015) 732–750.

[13] Y. Su, H. Li, H. Ma, J. Robertson, A. Nathan, Controlling surface termination and facet orientation in Cu2O nanoparticles for high photocatalytic activity: a combined experimental and density functional theory study, ACS Appl. Mater. Interfaces 9 (2017) 8100–8106.

[14] D. Tahir, S. Tougaard, Electronic and optical properties of Cu, CuO and Cu2O studied by electron spectroscopy, J. Phys. Condens. Matter 24 (2012) 175002.

[15] J. Zhang, J. Liu, Q. Peng, X. Wang, Y. Li, Nearly monodisperse Cu2O and CuO nanospheres: preparation and applications for sensitive gas sensors, Chem. Mater. 18 (2006) 867–871.

[16] R. Wick, S.D. Tilley, Photovoltaic and photoelectrochemical solar energy conversion with Cu 2 O, J. Phys. Chem. C 119 (2015) 26243–26257.

[17] J. Luo, L. Steier, M.K. Son, M. Schreier, M.T. Mayer, M. Grätzel, Cu2O nanowire photocathodes for efficient and durable solar water splitting, Nano Lett. 16 (2016) 1848–1857.

[18] M. Schreier, J. Luo, P. Gao, T. Moehl, M.T. Mayer, M. Grätzel, Covalent immobilization of a molecular catalyst on Cu2O photocathodes for CO2 reduction, J. Am. Chem. Soc. 138 (2016) 1938–1946.

[19] W.C. Huang, L.M. Lyu, Y.C. Yang, M.H. Huang, Synthesis of Cu2O nanocrystals from cubic to rhombic dodecahedral structures and their comparative photocatalytic activity, J. Am. Chem. Soc. 134 (2012) 1261–1267.

[20] Q. Hua, D. Shang, W. Zhang, K. Chen, S. Chang, Y. Ma, Z. Jiang, J. Yang, W. Huang, Morphological evolution of Cu2O nanocrystals in an acid solution: stability of different crystal planes, Langmuir 27 (2011) 665–671.

[21] Y. Xu, H. Wang, Y. Yu, L. Tian, W. Zhao, B. Zhang, Cu2O nanocrystals: surfactant-free room-temperature morphology-modulated synthesis and shape-dependent heterogeneous organic catalytic activities, J. Phys. Chem. C 115 (2011) 15288–15296.

[22] L. Zhang, J. Shi, M. Liu, D. Jing, L. Guo, Photocatalytic reforming of glucose under visible light over morphology controlled Cu2O: efficient charge separation by crystal facet engineering, Chem. Commun. 50 (2014) 192–194.

[23] H. Xu, W. Wang, W. Zhu, Shape evolution and size-controllable synthesis of Cu2O octahedra and their morphology-dependent photocatalytic properties, J. Phys. Chem. B 110 (2006) 13829–13834.

[24] H. Gao, J. Zhang, K. Liu, J. Yang, M. Wang, W. Wang, Time-dependent hydrothermal synthesis and self-evolution mechanism of Cu2O microcrystals, Mater. Charact. 71 (2012) 112–119.

[25] M. de A. Barbosa, G. da S.L. Fabris, M.M. Ferrer, D.H.M. de Azevedo, J.R. Sambrano, Computational simulations of morphological transformations by surface structures: the case of rutile TiO2 phase, Mater. Res. 20 (2017) 920–925.

[26] M.M. Ferrer, A.F. Gouveia, L. Gracia, E. Longo, J. Andrés, A 3D platform for the morphology modulation of materials: first principles calculations on the thermodynamic stability and surface structure of metal oxides: Co3O4 , α-Fe2O3 , and In2O3, Model. Simul. Mater. Sci. Eng. 24 (2016), 025007.

[27] J.P. Perdew, K. Burke, M. Ernzerhof, Generalized gradient approximation made simple, Phys. Rev. Lett. 77 (1996) 3865–3868.

[28] G. Kresse, J. Furthmüller, Efficient iterative schemes for ab initio total-energy calculations using a plane-wave basis set, Phys. Rev. B. 54 (1996) 11169–11186.

[29] G. Kresse, J. Hafner, Ab initio molecular-dynamics simulation of the liquid-metal–amorphous-semiconductor transition in germanium, Phys. Rev. B. 49 (1994) 14251–14269.

[30] G. Kresse, D. Joubert, From ultrasoft pseudopotentials to the projector augmented-wave method, Phys. Rev. B. 59 (1999) 1758–1775.

[31] R. Restori, D. Schwarzenbach, Charge density in cuprite, Cu2O, Acta Crystallogr. Sect. B Struct. Sci. 42 (1986) 201–208.

[32] J. Andrés, L. Gracia, A.F. Gouveia, M.M. Ferrer, E. Longo, Effects of surface stability on the morphological transformation of metals and metal oxides as investigated by first-principles calculations, Nanotechnology 26 (2015) 405703.

[33] G. Wulff, XXV. Zur Frage der Geschwindigkeit des Wachsthums und der Auflösung der Krystallflächen, Zeitschrift Für Krist. - Cryst. Mater. 34 (1901).

[34] K. Momma, F. Izumi, VESTA 3 for three-dimensional visualization of crystal, volumetric and morphology data, J. Appl. Crystallogr. 44 (2011) 1272–1276.

[35] Z. Gao, W. Sun, Y. Hu, Mineral cleavage nature and surface energy: anisotropic surface broken bonds consideration, Trans. Nonferrous Metals Soc. China 24 (2014) 2930–2937.

[36] F. Ma, K.W. Xu, Using dangling bond density to characterize the surface energy of nanomaterials, Surf. Interface Anal. 39 (2007) 611–614.

[37] M.D. Susman, Y. Feldman, A. Vaskevich, I. Rubinstein, Chemical deposition of Cu2O nanocrystals with precise morphology control, ACS Nano 8 (2014) 162–174.

[38] M.J. Siegfried, K.S. Choi, Elucidating the effect of additives on the growth and stability of Cu2O surfaces via shape transformation of pre-grown crystals, J. Am. Chem. Soc. 128 (2006) 10356–10357.